Influence of pressure, temperature, and pore fluid on the frequency-dependent attenuation of elastic waves in Berea sandstone

Stephen G. O'Hara

Phillips Petroleum Company Research Center, Bartlesville, Oklahoma 74004

The effects of pore fluid, effective stress, pore fluid pressure, and temperature on the frequency dependence of elastic wave attenuation in Berea sandstone are interrelated in a series of systematic experiments. The attenuation of both the extensional and torsional modes of cylindrical samples of the sandstone is measured on the frequency range 3—30 kHz. To simulate conditions within the earth, the sandstone is subjected to confining stress to 70.0 MPa and temperature from 24.0 °C to 120.0 °C. Confining pressure and pore fluid pressure are varied independently. Data for two different pore fluids, brine and *n*-heptane, suggest that a scaling law exists for the pressure and temperature dependence of the attenuation in terms of the pore fluid. The logarithmic decrement of the sandstone is almost frequency independent in a vacuum evacuated sample, but shows a linear frequency dependence, once the sample is saturated. Extrapolation of this linear trend to low frequencies suggests that the decrement in fluid-filled sandstone is effectively frequency independent at seismic frequencies (< 100 Hz). The frequency dependence becomes more pronounced as either the effective stress or the temperature is decreased. When the difference between the external stress on the sandstone and the pore fluid pressure is large, the attenuation depends only on the effective stress and is relatively temperature independent. But at low effective stress, the attenuation increases linearly with increasing pore fluid pressure and decreases linearly with increasing temperature. While a specific model is lacking, the attenuation process is apparently influenced most strongly by chemical processes at the pore fluid-matrix interface accompanied by subtle changes in the sandstone matrix dimensions.

I. INTRODUCTION

Elastic wave measurements are one of the most commonly used geophysical techniques for studying the structure of the earth and exploring for commercial hydrocarbon deposits. From one point of view, earth attenuation effects are a limiting factor in such measurements, particularly at higher frequencies. From another, earth attenuation is an additional observation of the physical properties of buried rock. Unfortunately, the physical basis for attenuation is not understood. Frequently, the attenuation is explained in terms of a combination of proposed mechanisms, but these mechanisms are difficult to quantify and compare with the experimental data. And while a sizable number of bench-top attenuation measurements are reported in the literature, measurements on rock with full-scale simulation of conditions found inside the earth are much less common.

The present work was undertaken in an attempt to study several factors believed to be important in the attenuation process in one series of measurements. Measurements are made of the frequency-dependent attenuation and velocity on the range 3—30 kHz in a clean sandstone. As the sandstone is rather isotropic, only two independent elastic wave modes need be studied. Two fluids, a brine solution and normal heptane, are used as pore fluid in a parallel series of measurements. These two fluids offer some variation in the chemical interaction between the pore fluid and the sandstone grains which may be important to the attenuation process. The confining stress applied to the rock, the pore fluid pressure, and the rock temperature are all varied systematically for both fluids to simulate a variety of conditions within the earth.

A. Measures of earth attenuation

A wide variety of field and laboratory experiments indicate that the amplitude of an elastic wave traveling through rock follows an exponential absorption law. So with distance, the amplitude of a traveling wave decays:

$$u(x) = u_0 e^{-\alpha x}, \tag{1}$$

where u_0 is a reference amplitude. The form (1) presumes the rock medium is linear and homogeneous. The attenuation coefficient α depends on the frequency and for a particular elastic wave mode is known to depend on the type of rock and thermodynamic conditions imposed on the rock.

Many laboratory measurements of attenuation in rock including those to be reported here are made on small laboratory samples set into resonant oscillation. Usually it is sufficient to assume that the displacement $q(t)$ of such a sample is that of a damped harmonic oscillator:

$$q(t) = q_0 e^{-\delta t/\tau} \cos\left[\frac{2\pi t}{\tau} + \beta\right]. \tag{2}$$

The constants q_0 and β are obtained from initial conditions. The measure of energy loss in such a sample is the logarithmic decrement δ,

$$\delta = \ln \left[\frac{q(t)}{q(t+\tau)} \right] , \qquad (3)$$

obtained by measuring the amplitude of sample vibrations (usually the peak amplitude) at two times separated by one period of oscillation τ. If energy losses in the rock are not too great, the decay of standing waves in a resonating sample measures the same physical process responsible for absorption of energy from a traveling wave of the same frequency. Then, for $\delta < 0.3$, δ and α can be related:[1]

$$\alpha = \frac{f\delta}{V} , \qquad (4)$$

where V is the phase velocity and f is the frequency of the elastic wave.

B. Experimental considerations

In these experiments thermodynamic conditions impressed on the sandstone sample will serve as the independent variables. Then patterns in the measured attenuation and velocity as determined by changing pressure and temperature can be compared with corresponding changes in physical and chemical properties of the sandstone. The experiments are not designed to provide specific tests for proposed models for attenuation. Rather, the variables selected are based on trends appearing in previous field and laboratory studies on rock.

As the absorption law (1) is appropriate only for a linear elastic medium, a preliminary consideration is the range of strain amplitudes for which this law can be applied in rock. An indication of nonlinear behavior is the initiation of amplitude dependence in the measured attenuation coefficient with increasing strain amplitude. Several investigators have been able to show that various kinds of rock behave in a linear fashion until strain amplitudes exceed about 10^{-6}. In Berea sandstone, Tittman[2] reports classical anharmonic behavior in resonating samples beginning at about these strain amplitudes. In a more complete study involving sandstone, Winkler, Nur, and Gladwin[3] examined the effect of pore fluid saturation and static stress on the amplitude dependence. Large strain amplitude measurements may yield important data about basic attenuation mechanisms. But precautions were taken to limit strain amplitudes in the present study to the amplitude independent range.

As regards the frequency dependence of the attenuation, the consensus of the experimental evidence until rather recently was that the decrement of earth materials is independent of the frequency. Or, from (4), the attenuation of traveling waves increases linearly with the frequency. This opinion seems to be based on a sizable number of measurements on "air-dry" laboratory samples made under room conditions and an interpretation of the few field data sets on attenuation which exist. However, theoretical attempts to incorporate the frequency dependence in a linear attenuation model have been unsuccessful. A linear theory seems required from the amplitude independence of the attenuation and the general impression that the principle of superposition holds in observations of low-amplitude seismic events.

In fact, findings from laboratory measurements of attenuation suggest a complicated frequency dependence related to pore fluid properties. Born[4] found that dry rock showed a frequency-independent decrement. But in fluid saturated rock the decrement was found to increase with frequency to a degree depending on the particular pore fluid used. In more recent work, Tittman and co-workers[5] describe careful measurements on rock in which the last vestiges of fluid are removed by vacuum evacuation of the pore space. During evacuation the decrement can decrease orders of magnitude below that observed at room conditions. In such a state the attenuation appears to be controlled by the remaining pore fluid adsorbed onto the matrix grains. Clark and co-workers[6] demonstrate that this attenuation depends on the mass of the adsorbed fluid and the adsorption characteristics of the fluid to the matrix material. But regardless of magnitude, the measured decrement in vacuum evacuated rock appears to be frequency independent. Experiments of Pandit and King[7] and Murphy[8] suggest that as fluid is added to evacuated rock, a transition from frequency-independent to frequency-dependent behavior takes place. This transition seems to be associated with the accumulation of sufficient adsorbed pore fluid that macroscopic fluid droplets begin to form at selected sites within the pore space.

In the limit of no fluid, Mason and co-workers[9] suggest that the attenuation in dry rock is controlled by dislocation mechanisms at the surface of matrix grains and cement. Their model accompanied by some high-frequency (> 10 kHz) data indicates this decrement is not frequency independent but increases to a maximum occurring at ultrasonic frequencies. The attenuation due to internal friction losses inside matrix grains is probably much smaller and of the order of losses in solid mineral crystals.

In general, the frequency dependence and the pressure and temperature dependence of the attenuation have not been correlated. Measurements using spectrum analysis of ultrasonic pulses indicate the decrement in brine-saturated Berea sandstone is frequency independent at low ultrasonic frequencies.[10] In rather limited tests at lower frequencies (≈ 5 kHz) and confined to low effective stress (< 10 MPa), Winkler[11] reports a frequency-dependent decrement in water-saturated sandstone. Tittman and co-workers[12] report a lower decrement in water-saturated sandstone near seismic frequencies (≈ 100 Hz) than at high frequency (≈ 7 kHz) over a wide range of pressures. Wyllie, Gardner, and Gregory[13] find a quadratic frequency dependence for the attenuation at frequencies near 20 kHz and support for the theory of Biot.[14] But Gardner, Wyllie, and Droschak[15] report a frequency-independent decrement in fluid-saturated sands and glass bead packs in the same general frequency range.

Studies of the pressure dependence of the attenuation are usually parametrized in terms of the external static stress applied to the sample and the sample pore fluid pressure. An additional thermodynamic variable which should be considered is the effective stress

$$p_{\text{eff}} = p_{\text{ext}} - c p_f . \qquad (5)$$

Regarding these three stresses as a simulation of the conditions of burial of a sandstone within the earth, the exter-

nal static stress p_{ext} is taken to simulate the weight of overburden. The fluid pressure p_f simulates the hydrostatic head. Then p_{eff} is the net stress compressing the sandstone grains at sites of grain contact. Usually $c = 1.0$ in sandstone but may take on values $0.7 < c < 1.0$ in various other lithologies.[16] Typical studies of the pressure dependence contain data on air-dry and on water-saturated samples and may include data for partial saturation of the pore space. It is generally assumed that the velocity and attenuation scale with a simple effective stress law ($c = 1.0$). In all cases the attenuation decreases with increasing effective stress. The changes are somewhat logarithmic, with large changes at low effective stress and an attenuation relatively independent of pressure at large effective stress.

Measuring the attenuation and velocity as a function of the effective stress will help determine whether (5) is an appropriate expression of the concept. But beyond this, such a procedure will correlate the attenuation with the pore fluid pressure without changing the dimensions of the rock matrix. While the attenuation (and velocity) change logarithmically with stress, the density changes very slowly. Apparently, elastic properties of rock are quite sensitive to changes in the volume of smaller pore openings in the matrix. Measurements as a function of the effective stress offer some potential for separating the effects of these geometric factors in the attenuation process from the influence of the pore fluid.

The temperature dependence of the attenuation should also reflect both pore fluid effects and matrix dimensional changes. For the range of temperature for which sedimentary rock is found in the earth, dimensional changes in a sandstone matrix are very subtle. Nonetheless, the sensitivity of the attenuation to stress-induced dimensional changes argues for some temperature-dependent effects. At high temperatures corresponding to depths deep within the earth's crust, phase changes in matrix mineral grains can produce dramatic changes in attenuation.[17] But with the exception of a recent measurement,[18] the temperature dependence of attenuation at shallow depths has been neglected.

Berea sandstone is selected for the present study. This sandstone is widely used throughout the petroleum industry in reservoir engineering simulations so that data exists on its various physical properties. Berea is available in sample lots which are notoriously homogeneous, isotropic, and uniform in porosity and permeability. The matrix is primarily quartz and low in clay content so that any effects that interstitial clay might have on the attenuation will be minimized. (See the Appendix for a further description of Berea.) And for purposes of comparison, a number of studies already exist on several aspects of attenuation in Berea.

The present measurements attempt to unify observations simulating conditions within the earth with that work suggesting an adsorption mechanism for attenuation in vacuum evacuated rock. The choice of both brine solution and n-heptane offers some variety in physical properties of the pore fluid over the pressure and temperature range of this experiment (0—70 MPa, 24 °C—120 °C). But the two fluids also represent a significant difference in

fluid adsorption properties and the manner in which the sandstone matrix is wetted by the pore fluid. The brine used was a 10 000-ppm sodium chloride solution. The salt in the solution should reduce any effects due to swelling of hygroscopic clay minerals within the Berea matrix. The n-heptane used was reagent grade.

II. EXPERIMENTAL METHOD

A. Resonant rod

The elastic properties of an isotropic solid can be conveniently determined from the normal modes of vibration of a right circular cylinder made of that solid. This classical problem has been studied extensively both theoretically and experimentally,[1,19] so only a few relevant features are presented here. In principle, an infinite number of normal modes of vibration of a cylinder exist, but the experimental technique is contrived to excite either one of two first-order modes.

The first mode used is known variously as the extensional, rod longitudinal, or Young's modulus mode. In cylindrical coordinates, with the origin at one end of the cylinder and with the z axis and cylinder axis coinciding, the displacement for the extensional standing wave is

$$u_r = \mathcal{U}_n(r,\theta)\sin(n\pi z/L)\cos(2\pi f_n t + \epsilon) ,$$

$$u_\theta = 0 , \qquad\qquad\qquad\qquad\qquad\qquad (6)$$

$$u_z = \mathcal{W}_n(r,\theta)\cos(n\pi z/L)\cos(2\pi f_n t + \epsilon)$$

for each harmonic n. This solution applies for a cylinder of length L and diameter $2a$ for $L \gg a$. Initial conditions are contained within $\mathcal{U}_n$, $\mathcal{W}_n$, and ϵ. The harmonic frequencies at which resonances occur are

$$f_n = \frac{n}{2L}\left[\frac{E}{\rho}\right]^{1/2}\left[1 - \frac{\sigma^2\pi^2 n^2 a^2}{4L^2}\right] , \qquad (7)$$

where E is the Young's modulus, σ is Poisson's ratio, and ρ is the density of the cylinder. So for the fundamental harmonic, the mode phase velocity is

$$V_Y = 2Lf_1 \approx \left[\frac{E}{\rho}\right]^{1/2} . \qquad\qquad (8)$$

Samples were prepared so that $L/a > 30$ and practical considerations restricted the number of harmonics which could be studied. So dispersion in the velocity calculated from higher harmonics was expected to lower the velocity (8) by less than 1% for $n < 10$.

The other mode used was the torsional or rod shear mode. The displacement for the standing torsional wave is all rotational about the cylinder axis:

$$u_r = 0 ,$$

$$u_\theta = \mathcal{V}_n(r,\theta)\cos(n\pi z/L)\cos(2\pi f_n t + \epsilon) , \qquad (9)$$

$$u_z = 0$$

for each harmonic n. Initial conditions are specified by $\mathcal{V}_n$ and the phase ϵ. The frequencies at which harmonics occur are given by

$$f_n = \frac{n}{2L}\left[\frac{\mu}{\rho}\right]^{1/2} , \tag{10}$$

so that the mode is dispersionless with velocity

$$v_s = \frac{2Lf_n}{n} = \left[\frac{\mu}{\rho}\right]^{1/2} . \tag{11}$$

To introduce attenuation, the usual procedure is to make the frequency complex:

$$2\pi f = 2\pi v + iv\delta . \tag{12}$$

Substitution into (6) and (9) produces displacement coordinates of the form (2). This procedure does make the velocities (8) and (11) of the form

$$V = \frac{2Lv_n}{n}\left[1 + \frac{i\delta_n}{2\pi}\right] . \tag{13}$$

But this study considers $\delta/2\pi < 0.05$ and the effect of the attenuation on the velocity should be negligible. The procedure (12) is equivalent to assuming the cylinder is a Voigt solid at each frequency and then allowing δ to be frequency dependent in accordance with the experimental data.

B. Sample preparation

Sample cylinders were prepared from a lot of Berea believed to be uniform in porosity and permeability. Samples were cored and cut to length using diamond-studded tools. End faces of the sample were made parallel to better than 0.01 cm and perpendicular to the cylinder axis to at least 5×10^{-3} rad. To satisfy the requirement $a \ll L$, samples were made as long as the pressure apparatus and drying oven used could conveniently accommodate. All samples have a diameter of (2.22 ± 0.01) cm and a nominal length of 38 cm. Water cooling was used throughout preparation.

Following the cutting procedure, each sample was baked dry at 105 °C—115 °C for at least 12 hours in an oven open to the atmosphere. After cooling, samples were jacketed with 0.13-mm-thick copper foil. This jacket serves to isolate the rock pore space so that the pore fluid pressure and the external stress applied to the sample can be varied independently. Jacket seams were sealed with lead-tin alloy solder. To admit fluid to the sample pore space and control the pore fluid pressure, a 1.59-mm-diam stainless-steel high-pressure line was soldered into a hole through the jacket. This hole was drilled into the side wall of the jacket at a point equidistant from the two sample ends. Thus the fluid line enters the sample in a nodal plane for odd harmonics of either the extensional or the torsional mode. Finally, the sample was subjected to at least 20 MPa effective stress to test jacket integrity against leaks. The jacket being sound, this test serves to seize the copper foil onto the sandstone.

Jackets prepared in this manner proved extremely reliable. Experiments of more than two months' duration became possible. During this time, samples could be repeatedly cycled from room conditions to temperatures of

120 °C and effective stress of 80 MPa. Jacket failure, when this occurred, usually took place at a solder joint and occurred more frequently at high temperatures. This might be expected since the lead-tin solder used has a much lower melting temperature and a resulting higher creep rate than does the copper foil. Jackets of a thinner 0.08-mm foil were tried, but these proved to be unreliable for effective stress greater than about 50 MPa.

C. Pressure apparatus

The pressure apparatus must function so that the sample confining stress, pore fluid pressure, and sample temperature can all be varied independently. At the same time this simulation of the conditions within the earth must not severely restrict measurements on the vibrating sample. And the apparatus must be constructed so as to minimize the hazards inherent in high-pressure experimentation. The resulting design is represented schematically in Fig. 1.

The confining stress is produced by enclosing the jacketed sample in a vessel in which helium is the pressurizing medium. Helium is used primarily to minimize damping of the sample vibrations. Confining stress is measured with a transducer gauge which utilizes a strain gauge sensor in a four arm resistance bridge. (A list of the specific instruments used is provided in Table I.) Calibration by the manufacturer and tests of the gauge against secondary standards both indicate an accuracy better than ± 0.3 MPa. This type of gauge can show long-term zero drift. So provision was made to isolate the gauge from the pressure vessel so that the gauge could be periodically vented and rezeroed on a two-to-three-day basis.

The fluid pressure in the sample pore space is controlled through the miniature pressure line soldered into the side of the sample jacket. This line is connected through one end closure of the sample pressure vessel to a system which is also used to vacuum evacuate the sample and to introduce pore fluids into the sample. The vacuum system consists of a mechanical pump, a liquid nitrogen cold trap, and a precision bourdon gauge, all protected against overpressure. Once the pore fluid is loaded into
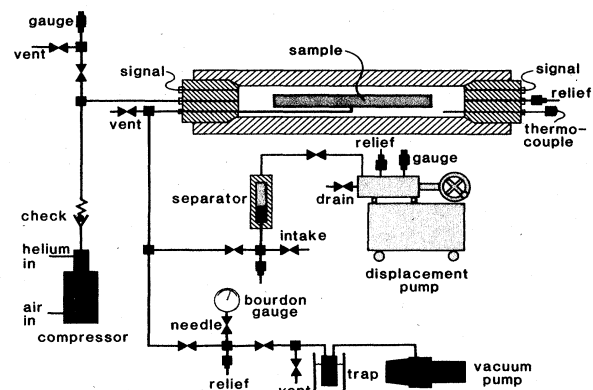
FIG. 1. Pressure apparatus used to subject sandstone samples to elevated temperatures and hydrostatic confining pressures and to regulate the sample pore fluid pressure.

TABLE I. Experimental apparatus.

Pulse generator	Tektronix PG508
Function generator	Tektronix FG504
Power amplifier	Krohn-Hite DCA-10
Signal amplifier	Tektronix AM 502
Bandpass filter	Tektronix AF 501
Oscilloscope	Tektronix 7603
	with 7B53A time base
	7A13 comparator amplifier
	7D15 counter-timer
Pressure gauges	Autoclave Engineers DPS-0202
	digital indicator with transducers
Vacuum gauge	Heise bourdon tube absolute pressure
	0—200 kPa
Thermometers	Copper-constantan thermocouple
	with Fluke 2170A monitor
	Fluke 2162A comparator
Gauge monitor	Hewlett-Packard 3467A logging multimeter

the sample, the vacuum system is disconnected and pressure is controlled by a positive displacement pump operating through a separator. Pore fluid pressure is measured with a second transducer gauge mounted on the displacement pump. As for the first gauge, this second gauge can be rezeroed by isolating the displacement pump from the pore fluid system.

The temperature of the sample is controlled by heating the sample pressure vessel with silicone tapes wrapped about the vessel exterior. Regulation of the heating tape current proved unnecessary as a vessel mass greater than 100 kg provides temperature stability of $\pm 0.4\,°C$. A copper-constantan thermocouple probe sealed into one end closure of the pressure vessel estimates the sample temperature from that of the high-pressure helium gas. The probe is sheathed to prevent shifts in calibration caused by the effect of pressure on the thermocouple junction. The probe calibration accuracy is $\pm 0.4\,°C$. To determine the reliability with which the probe measured the sample temperature, probe readings were compared with a second thermocouple placed at various sites within the pressure vessel. With cell pressure at 1 atm, the thermal gradients within the cell were no worse than $2.0\,°C$ at $120\,°C$.

D. Transducers

Measurements of the resonant vibrations of sandstone samples are made using miniature piezoelectric transducers mounted on opposite ends of the sample. The polarization and size of the transducers are selected to match the boundary conditions of each of the vibrational modes of the sample. The transducer on one end serves to drive the sample into oscillation in response to an applied sinusoidal electric signal. The transducer on the opposite end detects the sample vibrations, producing an electrical signal used to record the sample velocity and attenuation.

For the longitudinal mode, small compressional transducers are mounted concentric with the sample cylinder axis. The transducers are cylinders of PZT 5 ceramic 0.64 cm in diameter and 0.32 cm thick. Calculations using (6) show that the displacement component u_z across the sam-

ple end face is relatively independent of the radius for the fundamental mode. But for higher harmonics, the same calculations show the end faces distort nonuniformly. Experiments confirm that the transducers must be somewhat smaller than the sample diameter to obtain pure harmonics of the extensional mode.

For the torsional mode, the transducers are constructed of six pie-shaped sections of shear polarized PZT 5 plates arranged in a circular fashion. The composite transducer is an annulus of outside diameter 2.0 cm and inside diameter 0.7 cm. The shear sections are polarized so that an electric field applied perpendicular to the cylinder axis of the annulus produces a torque in the composite transducer. While such a transducer only approximately satisfies the boundary conditions for the displacement u_θ in (9), the actual measurements show this simple design produces very clean harmonics.

Transducers are applied to the jacketed sample after the jacket has been formed to the sandstone while pressure testing for jacket leaks. This assures good traction between the transducer and the underlying sandstone. Emerson Cumming Eccobond 66C epoxy is applied to make each transducer end surface conducting and cement the transducer to the jacketed sample. Signal leads are No. 36 magnet wire and signal ground is made through the sample jacket and pore fluid line.

E. Electronic apparatus and technique

With the sample transducers described, the determination of the mechanical properties of the sandstone sample becomes a precision electrical measurement. Figure 2 is a block diagram of the audio-frequency electronics used to make these measurements. For each measurement the sample is driven into oscillation at a resonant frequency, then allowed to vibrate in free decay. The signal applied to the driver transducer is a sinusoidal voltage produced by the function generator and amplified to a level of 10—100 V. The duration of this signal is determined by the pulse generator which simultaneously gates the function generator and triggers the oscilloscope main time
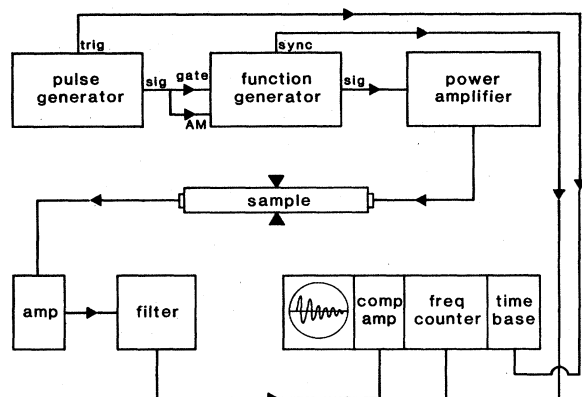
FIG. 2. Block diagram of electronic apparatus used for resonant rod measurements.

FIG. 3. Cross section showing sample mounted within hollow cylinder of acoustic insulation. Sample is clamped by three mounting screws placed 120° apart on the circumference of an aluminum annulus which serves as the central section of the insulating cylinder. Only one of the mounting screws is visible in the section.

base. The pulse generator also amplitude modulates the signal with a trapezoidal gate to produce a taper at the beginning and end of the pulse. This taper is essential to reduce high-frequency components in the signal applied to the driver transducer. Such components produce ultrasonic echoes in the rock sample which complicate the measurement of the attenuation. In practice these echoes limit the number of overtones which can be used for measurements, particularly for large values of the attenuation.

The velocity is calculated from either (8) or (11) by measuring the frequency of the resonance with a counter-timer plug-in module in the oscilloscope. For given conditions of temperature and pressure, each harmonic in turn is located by tuning the frequency of the function generator until a maximum detector signal is observed. This tuning procedure by itself gives rise to an uncertainty in the measured frequency of at most 0.1%. Error contributed by the counter-timer is negligible. The sample length used to calculate the velocity is not corrected for the effects of pressure and temperature. Neglecting corrections based on the thermal expansion[20] or the compressibility[21] of Berea introduces an error in the velocity of less than 0.5%. For any given measurement, slight variation (< 0.5%) is evident in the calculated velocity depending on the harmonic chosen to make the calculation. This variation may reflect slight inhomogeneity in the jacketed sample as well as subtle effects of transducer loading.

The attenuation is calculated from measurement of the time rate of decay of the peak detector signal after termination of the driver signal. The measurement is made with a comparator amplifier plug-in module in the oscilloscope. The data is fitted to the exponential envelope function of (2) by the method of least squares to obtain the decrement. Large numbers of trials ($\approx$ 30) of the measurement procedure made at selected data points and assumed to be normally distributed show a standard deviation in the decrement in the range 1—3 %.

F. Restrictions and corrections applied to the data

Measurement of the attenuation and velocity is subject to a number of sources of error which act in a systematic
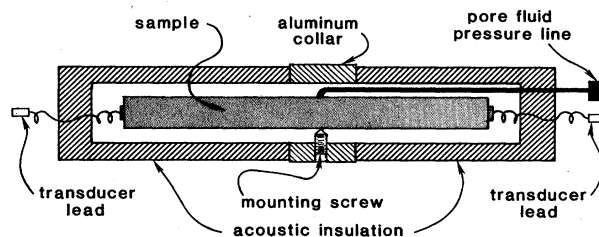
and predictable manner. Included are transducer performance, mechanical coupling between the resonant sample and the apparatus, and interaction between sample and jacket. The effect of these factors can be minimized by careful design and good technique. But these factors are also ultimate physical limitations which in some cases restrict the range of variables studied and in others require appropriate corrections to the data.

As a result of experiments to gauge the effect of the apparatus on the measurements, a simple design emerged for mounting the sandstone samples. (See Fig. 3.) The sample is clamped at its midpoint in an aluminum collar with three set screws 120° apart around the sample circumference. Thus the sample is free to vibrate for odd harmonics of either the extensional or torsional mode. The sample is encased in a cylinder of acoustic tile insulation which absorbs acoustic waves generated by the sample motion in the gas confining medium of the pressure vessel. While designing this mounting arrangement, aluminum rods were used as samples to optimize the mount design. Decrements in these metal rods measure less than 1×10^{-4}, so changes in the measured rod velocity and attenuation could be attributed to the mounting arrangement. For the set screw mount and the transducers selected, some variation in attenuation was found to occur for different odd harmonics in the aluminum. But the largest losses were $(2-3) \times 10^{-4}$, and these are negligible compared to losses observed in fluid-saturated sandstone samples.

The performance of the transducers is best understood by examining the vibrational frequency spectrum of a resonating sample. The process is illustrated in Fig. 4. A continuous sinusoidal signal of constant amplitude but variable frequency is impressed on the driver transducer. The resulting detector transducer signal is rectified so that the magnitude of the transducer response can be displayed as a function of the driver transducer frequency. The detector response has been linearized with a logarithmic amplifier (note vertical scale). Shown is the response obtained from a jacketed Berea sample saturated with brine and vibrating in the extensional mode. To eliminate high-frequency transducer noise (> 50 kHz), the signal was filtered with an active narrow-band-pass filter ($Q = 5$) whose band center frequency coincided with the
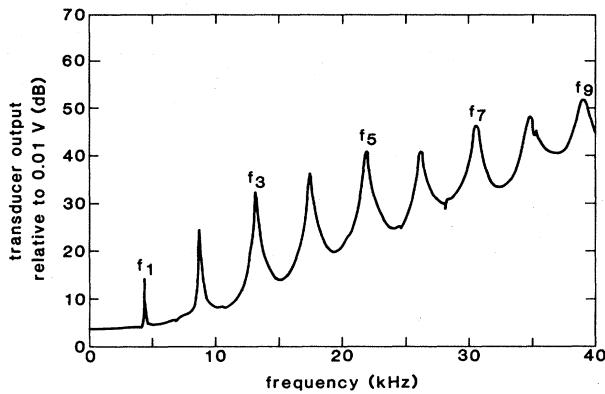
FIG. 4. Vibrational spectrum for the extensional rod mode of a brine-saturated Berea-sandstone sample with confining and pore fluid pressures at 0.1 MPa and temperature of 24.0 °C. The spectrum represents the rms average of the detector transducer output when a continuous sinusoidal voltage of constant amplitude is applied to the driver transducer. The vertical scale is the output after logarithmic amplification. The horizontal scale represents the driver transducer frequency swept over a range 2—40 kHz. Odd harmonic resonances are labeled.

driver transducer frequency. For the even-numbered harmonics, the midpoint sample mounting arrangement might be expected to produce distortion or a large attenuation. Such distortion does occur, particularly for the lowest even-numbered resonances, but is frequently not pronounced, as in this example. Receiver transducer performance was studied in a series of experiments generating spectra such as Fig. 4. Conspicuous in the spectrum are the dramatic increase in the amplitude of successive harmonics and the gradual broadening of the resonances as the frequency increases. For either vibrational mode, the signal amplitude of successive harmonics was found to increase approximately as the square of the harmonic resonant frequency. Thus the transducers behave as accelerometers in which the transducer itself serves as the inertial mass. Performance of the extensional transducer compared favorably with that of a miniature calibrated accelerometer (Endevco 2250) within the operating range of the accelerometer (< 10 kHz).

Broadening of the harmonic resonances with increasing frequency is to be expected for a damped oscillator system. Assuming the harmonic spectrum represents linearly independent oscillators, the measured decrements average the decrements of the adjacent resonances with that of the resonance being measured. And the frequency dependence of the decrement weights the contribution of the adjacent resonances in this average. In the present experiments the decrement increases linearly with the frequency for the fluid-saturated sandstone. This produces an error which is actually largest for the fundamental resonance, since only harmonics at higher frequencies enter this particular average. For higher-order harmonics, in spite of the large decrements and the number of harmonics entering the average, the measured decrement is relatively close to the true decrement. For the largest decrements measured, $\delta = 0.1 - 0.2$, the decrement of the fundamental is

overestimated by 5%. Considering the limited amount of data obtained on the frequency dependence at such large values of the decrement, the data were not corrected for this error. For lower values of the decrement where the frequency dependence is more evident, errors are of the order of $1 - 2\%$ and are neglected.

By far the most important limitation on accurate measurement of the attenuation in the sample is the helium gas confining medium. The high-pressure gas damps the oscillation of the sample resulting in acoustic wave propagation in the helium. Browne and Pattison[22] have studied the effect of this damping on the extensional vibrations of a cylindrical sample for the fundamental resonance. Their findings may be extended to include the torsional mode and the effect for harmonics of both modes. For samples in helium gas, extensional mode energy loss is dominated by compression of the gas by sample strain normal to the cylinder side and end surfaces:

$$\delta = \frac{4\pi^2 a^2 \rho_{He}}{L\rho} \left[\frac{\sigma^2}{L} + \frac{v}{V_{He}} \right] \tag{14}$$

with

$V_{He} =$ helium velocity ,

$\rho_{He} =$ helium density ,

$\rho =$ sample density, and

$\sigma =$ sample Poisson's ratio .

Loss to the extensional mode due to viscous drag of the gas by strain tangential to the sample surfaces is negligible, even at the highest pressures for which measurements were made. And as losses to the torsional mode consist entirely of viscous drag, this mode in the sandstone is virtually unaffected by the high-pressure helium.

The damping decrement equation (14) clearly shows the advantage of using helium gas as a confining medium. And the decrement is reduced by using a sample of high-aspect ratio ($L \gg a$). Figure 5(a) illustrates the behavior of the damping decrement calculated for odd harmonics of a dry Berea sample. Obviously, the damping will be most noticeable on high harmonics at high pressure. For this calculation, helium density was interpolated from data of Kao and Kobayashi.[23] Velocity was interpolated from the ultrasonic velocity in helium measured by Pitaevskaya and Bilevich.[24] Elevated temperature in the helium will lower the calculated decrement slightly. Changes in the sandstone properties with temperature and pressure are only second-order effects in the calculation.

Figure 5(b) shows the decrement measured for this same jacketed sample after the sample pore space had been thoroughly evacuated. The solid lines are provided as an aid to the eye. The data primarily reflects the damping decrement and the loss in the dry rock itself $[(3-4) \times 10^{-3}]$. A small correction has been made for the effect of the sample jacket (see below). But the data also reveals the presence of cell resonances within the helium gas (organ pipe modes), notably in the first harmonic. The acoustic insulation surrounding the sample (see Fig. 3) serves to greatly reduce these coupled oscillator resonances but cannot completely eliminate them.
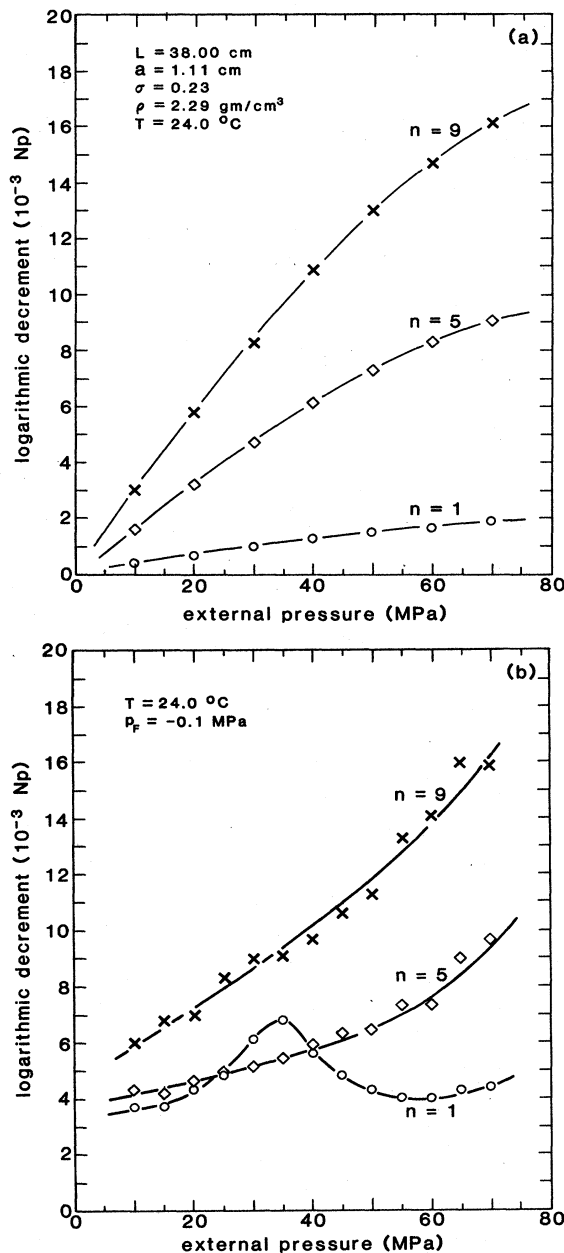
FIG. 5. Decrement of extensional mode of vacuum evacuated Berea sample vs helium gas confining pressure applied to the sample. (a) Calculated decrement from Eq. (14) for the harmonics $n = 1,5,9$ using those sample dimensions and properties listed in the figure. (b) Measured decrement for a Berea sample with the same dimensions used in the calculation for (a).

The data for the extensional mode have all been corrected for the damping decrement using (14), the sample dimensions, and the properties of the helium cited above. The sample density includes the density of the pore fluid specified as a function of pressure and temperature. The fluid density for water was interpolated from Kell and Whalley[25] and for n-heptane from Nichols, Reamer, and Sage.[26] Consideration was given to correcting the mea-

sured decrement of each saturated sample by measuring the decrement of the same vacuum dried rock at corresponding pressures and temperatures. But the increased risk of sample jacket failure in a prolonged experiment, hysteresis effects in the sample, and the volume of data required argued against this questionable improvement.

The final correction to be made to the data is for the effect of the sample jacket. The resonant rod is a composite oscillator consisting of a solid cylindrical core and a jacket including a hollow cylinder and two end cap sections. The core material, sandstone, possesses a relatively larger attenuation and smaller velocity than the copper jacketing material. The properties of an oscillator of this geometry and such relative mechanical properties have been treated by Gemant.[27] As applied here, the corrected velocity in the sandstone is

$$V_r^2 \approx \frac{4v_n^2 L^2 (m_s + m_j)/n^2 - C_j T_j}{m_s} \tag{15}$$

and the corrected decrement is

$$\delta \approx \frac{4v_n^2 L^2 (m_s + m_j)\delta_n}{n^2 m_s V_r^2} \tag{16}$$

in terms of the measured values v_n and δ_n for each harmonic n. The corrections depend on the masses of the sample and jacket m_s and m_j, as well as the volume of the jacket T_j. Both the extensional and the torsional modes are corrected using the appropriate elastic constant for copper, C_j, for each mode.[28] The effect of pressure and temperature on C_j are second-order effects in the correction.[29] Clearly, the high external pressure seals the jacket so tightly onto the sample that the jacket elastic properties are only approximately those of pure copper.

The jacket correction yields a velocity in the sample at most 5% lower than measured and a decrement at most 10% higher. But the correction to the decrement is multiplicative. Thus, to a good approximation, ratios of measured decrements for a given mode can be used to eliminate the effect of the jacket.

G. Hysteresis and repeatability

Inevitably when physical measurements are made on rock as a function of pressure and temperature, hysteresis effects appear in the data. Changes in thermodynamic conditions produce minute alteration of the rock fabric associated with localized stress relief and subtle volume changes in the sandstone matrix. And these alterations are not abrupt but take place over an extended period of time following a pressure or temperature change. The resulting sample creep is manifest as a logarithmic time-dependent drift in the measured attenuation and velocity. Thus no measurement is truly reproducible as each observation reflects the sample's past thermodynamic history.

Experience shows that hysteresis effects can be reduced somewhat by giving the sample an initial set. Thus before any pore fluid is injected, the jacketed sample is cycled to a pressure of at least 20.0 MPa. Hysteresis effects are most noticeable at low effective stress where the rate of change of volume with stress is largest. So once the set

has been obtained, the effective stress is not allowed to drop below 5.0 MPa. Because of creep, samples must be allowed to stand for times ranging from an hour to a day or more following changes in pressure and temperature. Again, the longest equilibrium times occur at low effective stress.

As discussed in the Introduction, the experiments are designed so that most measurements are made by varying a single thermodynamic variable at constant effective stress. This approach produces data which show the influence of each variable on the attenuation and velocity with a minimum amount of hysteresis in the measurements. Cyclic variation of the pressure and temperature shows that the velocity is reproducible to 2% and the decrement to 10% or better for constant effective stress. But comparison of data taken for samples with different thermodynamic histories indicates overall reproducibility is restricted to 5% in the velocity and 15—20% in the decrement.

III. RESULTS

A. Presentation of the data

The data are presented elsewhere in tabular form.[30] The data are divided into sets for the extensional and torsional wave modes and subdivided for brine or heptane pore fluid. Measurements were made at effective stresses of 5.0, 10.0, 20.0, 40.0, and 60.0 and temperatures of 24.0 °C, 70.0 °C, and 120.0 °C for all four cases so that comparisons could easily be made. Additional measurements, similarly subdivided, provide detail on the temperature dependence of the attenuation at low effective stress. From this tabulation selected data sets will serve to illustrate the effect of pore fluid, pressure, and temperature on the attenuation. Where appropriate the effect of these variables on the measured velocity is also considered.

B. Amplitude dependence

Using the calibration accelerometer, extensional mode strain amplitudes of $10^{-6}-10^{-7}$ were measured for peak drive transducer voltages. Strain amplitudes produced by the torsional transducers are assumed to be comparable. Thus nonlinear effects should not be present in the attenuation measurements. Several tests of the dependence of the measured decrement on the strain amplitude during the course of the experiments confirm this view. In each such test all harmonics were checked to confirm that the sample response and measurement technique were linear over the frequency range of the experiments. Then, as a practical matter, measurements were made at or near the peak driver amplitude to maximize the signal-to-noise ratio at the receiver transducer.

C. Attenuation in vacuum evacuated samples

As previously noted, all experiments were begun with the sample in a vacuum evacuated state. A typical sequence of events at the beginning stages of an experiment is illustrated in Fig. 6. Shown is the measured decrement
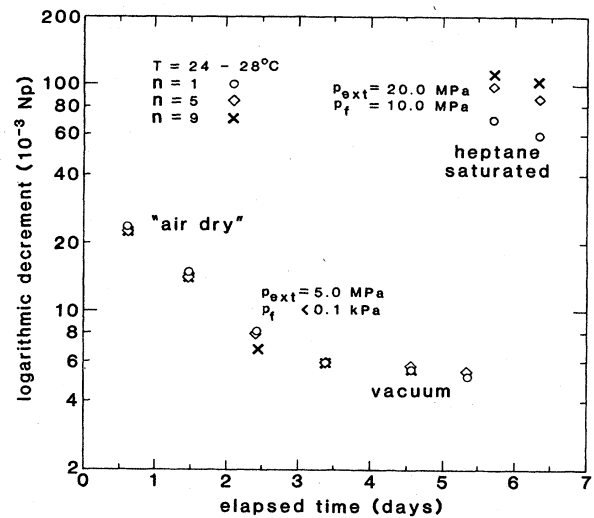
FIG. 6. Decrement for harmonics $n = 1,5,9$ showing the progression of changes from vacuum evacuation to fluid saturation during early stages of an experiment. Decrement is frequency independent and becomes relatively smaller as the sample is evacuated over a period of days. Once saturated, the decrement increases dramatically and becomes frequency dependent. See text for details as to sequence of events.

of the first, fifth, and ninth harmonics of the torsional mode in a jacketed sample at selected time intervals over the period of one week. These are raw data uncorrected for the effects of the jacket. The first measurement represents the decrement of an oven-dried sample mounted in the apparatus but with the pore space open to the laboratory environment. The sample is under a confining pressure of 5.0 MPa. The decrement is frequency independent and typical for that of an air dry sandstone. Subsequently, the sample is evacuated over a period of days and the decrement drops to 5×10^{-3}. Experience with many samples shows that continued evacuation does not produce appreciably lower decrements. On day 5, following a final datum taken for the vacuum state, the sample is allowed to siphon a pore fluid. Heptane was used in this example; brine produces similar results. The decrement immediately increases more than one order of magnitude and becomes frequency dependent. In this particular example, after several hours the cell and pore fluid pressures were adjusted to 20.0 and 10.0 MPa, respectively, to produce the datum on day 5 labeled "heptane saturated." Over the following 24 hours the sample creeps and finally stabilizes on the sixth day near the datum shown.

During initial stages of an experiment on the extensional mode, the sample behaves in an analogous fashion. However, the dry sample shows a slight frequency dependence which persists even after the sample has been vacuum evacuated for some time. This frequency dependence is characterized by an increase in decrement with harmonic number which is approximately linear. Saturation with either brine or heptane increases the attenuation as for the shear mode and makes the slight frequency dependence

become pronounced.

These observations and this procedure are in accord with the discussion on the importance of small amounts of volatiles on the attenuation. Values of the decrement obtained after vacuum evacuation are in the range $(4-8)\times10^{-3}$ with the torsional mode decrements lower than those obtained for the extensional mode. These decrements may represent the ultimate obtainable with the vacuum system used in the present experiments. On the other hand, other investigators find comparable results in sandstones using an apparatus designed specifically for vacuum measurements.[6] This "background" attenuation is probably due to mechanisms involving very tightly bound volatiles adsorbed to the matrix and dislocations within the matrix grains and cement. The present finding as to the relative magnitude of the extensional and torsional decrements is in qualitative agreement with measurements by Mason and co-workers[9] which attribute the decrement in dry rock to dislocation mechanisms.

Quite probably, the background attenuation is small compared to the total attenuation in a fluid-saturated sample regardless of the pressure or temperature. But the pressure dependence of the attenuation in a vacuum evacuated sample was tested for the torsional mode. As shown in Fig. 7, the decrement remains small over the range of confining stress used in the present experiments and is frequency independent. Data for 10.0,20.0, . . . ,70.0 MPa were taken for increasing pressure and data for 5.0,15.0, . . . ,65.0 MPa were taken for decreasing pressure. There is little obvious hysteresis except that the data for the fifth harmonic at 25.0 and 35.0 MPa are unaccountably spurious. A similar test for the extensional attenuation is not possible because damping of the confining gas dominates energy loss in the sample.
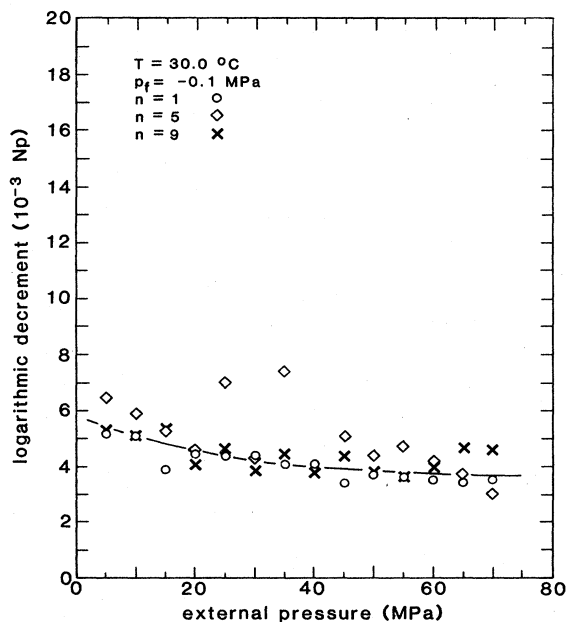
[See Fig. 5(b).] The effect of the temperature on the attenuation of the evacuated rock was not tested. But assuming the attenuation depends on the mass of fluid adsorbed within the rock matrix, the increasing temperature should reduce the adsorbed mass and, consequently, the background attenuation.

D. Effect of the pore fluid

It is evident in Fig. 6 that the attenuation in rock is dominated by mechanisms associated with pore fluid. The procedure of evacuating the rock is presumed to eliminate those mechanisms and provide a basis for comparison of the effect of different pore fluids on the attenuation. In fact, for the two fluids used in this study, the attenuation in the saturated rock is quite different. Figures 8(a) and 8(b) show a comparison of the dependence of the decrement on the effective stress for both elastic wave modes. The data were extracted for comparable conditions of pressure and temperature to highlight the effect of the pore fluid alone. Measurement frequencies for each mode were comparable for the two different saturation cases since samples were of similar length. Characteristically, the attenuation in the brine-saturated sample is roughly double that in the heptane-saturated sample. This pattern is sustained throughout the data for any given conditions of pressure, temperature, and elastic wave frequency. For both fluids, the decrement shows a dependence on the effective stress typical for a saturated sandstone.

The pressure dependence of the decrement is analogous to the well-known pressure dependence of the velocity in sedimentary rocks. For the decrements shown in Figs. 8(a) and 8(b), the corresponding velocities calculated from the sample resonance frequencies are plotted in Fig. 8(c). For a given effective stress, the velocity in the heptane-saturated sample is 5—6% faster than that in the brine-saturated sample. As for the effect of the pore fluid on the decrement, this effect on the velocity persists throughout the data, when comparisons are made for identical thermodynamic conditions.

E. Frequency dependence

As first noted in Fig. 6, the sample once saturated shows a decrement which increases with frequency. This is a general property exhibited by both modes for either pore fluid studied. Further, changes in the decrement caused by changes in the pressure and temperature are relatively larger as the frequency increases. An example is shown for the case of brine saturation in Fig. 9(a) for the extensional mode and in Fig. 9(b) for the torsional mode. Fluid pressure and sample temperature are fixed to suppress the effect of these variables. Both modes show fractional changes in decrement with frequency that increase with decreasing effective stress. The solid curves are intended only to group the data for the eye. The limited number of data points allow one to infer only a rough linear trend in the data. At low effective pressures, it becomes impossible to accurately determine the decrements for the higher-order harmonics. Interference from the small ultrasonic pulses produced by the driver transducer

FIG. 7. Decrement for harmonics $n=1,5,9$ of the torsional mode in vacuum evacuated Berea vs confining pressure applied to the sample.
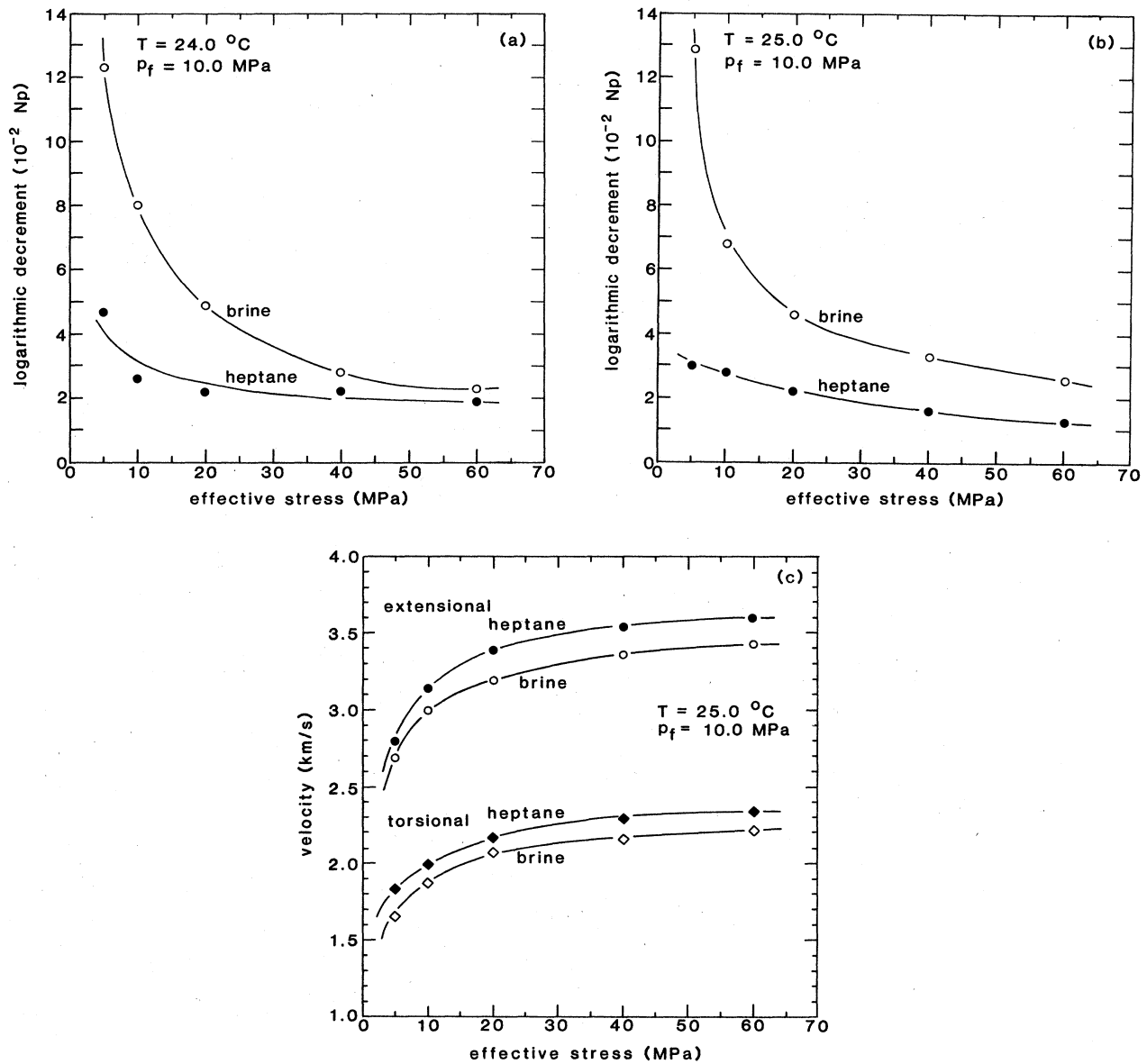
FIG. 8. Comparison of the decrement of brine-saturated Berea with that of heptane-saturated Berea vs the effective stress acting on the sandstone. Only first harmonic is shown. (a) Extensional mode. (b) Torsional mode. (c) Phase velocities for the corresponding decrements shown in (a) and (b). Comparisons made for pore fluid pressure of 10.0 MPa and a temperature of 24.0 °C—25.0 °C.

signal obscures the oscillations of the sample.

For the case of heptane saturation, the results for the frequency dependence for various effective stresses are exactly analogous except that the magnitude of the decrement is reduced proportionally as in Figs. 8(a) and 8(b). In discussions which follow of the effect of the pore fluid pressure and sample temperature on the decrement, examples will be given showing the frequency dependence in both heptane-saturated and brine-saturated samples. In the interest of simplicity only the behavior of selected harmonics will be displayed. It is to be understood, however, that the trend exhibited in Fig. 9 continues throughout the examples.

F. Effective stress law tests

To determine whether the attenuation follows an effective stress law, the decrement was measured as a function of external pressure applied to the sample for selected values of the effective stress. The effective stress was maintained throughout the course of an experiment by carefully adjusting the fluid pressure abreast of the external pressure. Measurements show the decrement does not depend simply on the difference between the external stress applied to a rock and the pore fluid pressure. Results for the extensional mode at 24.0 °C in a brine-saturated sample are shown in Fig. 10(a). Only the first
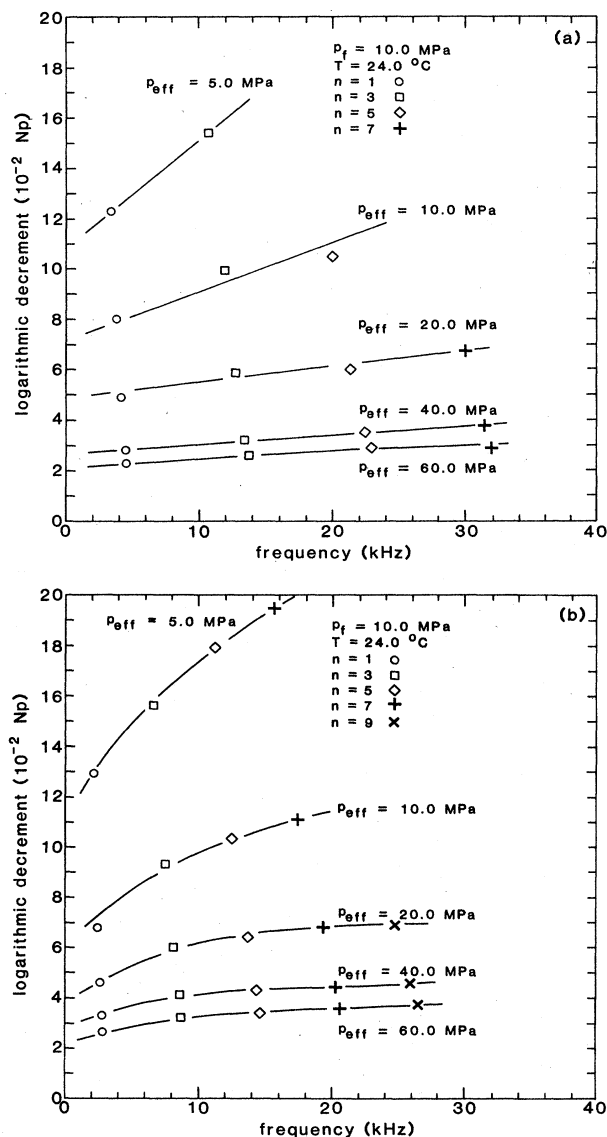
FIG. 9. Decrement in brine-saturated Berea vs frequency for various values of the effective stress applied to the sandstone. Comparisons made for pore fluid pressure of 10.0 MPa and temperature of 24.0 °C. Harmonics shown represent the maximum number at each effective stress for which measurements were considered reliable. (a) Extensional mode. (b) Torsional mode.

and third harmonics are shown. To gauge hysteresis, data at 10.0,20.0, . . . ,70.0 MPa were taken for rising external and fluid pressure and data for 15.0,25.0, . . . ,65.0 MPa were taken for falling pressures.

The significant feature of the data shown in Fig. 10(a) is the breakdown in the notion of the effective stress as the independent variable. The effect is most noticeable at low effective stress so that a gradual transition to a true effective stress law behavior takes place at high effective stress. As a result, the pressure dependence of the decrement illustrated in Fig. 8 and the frequency dependence

shown in Fig. 9 are particular to the fluid pressure chosen (10.0 MPa) at relatively low effective stress. As the experiments to test the effective stress law are contrived to hold the sample matrix dimensions constant, it is likely that the observed effect is controlled by the fluid pressure. The data suggest a dependence of the decrement on the effective stress plus a contribution that is approximately linear in the fluid pressure.

Predictably, similar behavior is evident in heptane-saturated Berea. Figure 10(b) shows a comparison of the measured extensional decrement at 5.0-MPa effective stress in brine-saturated Berea from Fig. 10(a) with corresponding data for heptane-saturated Berea. Data for three odd harmonics could be obtained in the case of the heptane. These particular data indicate the breakdown in the effective stress law is more pronounced at higher frequencies. This observation is suggested as well by other data in Figs. 10(a)—10(d).

For the torsional mode the breakdown is much less pronounced. Figure 10(c) shows the torsional decrement for conditions corresponding to those in Fig. 10(a) for the extensional mode. Only the first and fifth harmonics are shown. A departure from effective stress law behavior is evident only at the lowest effective stress. Figure 10(d) shows a comparison between the torsional decrements for the first three odd harmonics of both a brine-saturated sample and a heptane-saturated sample at 5.0 MPa.

The measured velocities follow the simple effective stress law as long as the decrement is not too large. But at low effective stress in brine-saturated samples, both modes show a subtle decrease in velocity as the pore fluid pressure increases.

G. Temperature dependence

In the examples chosen for purpose of illustration so far, the data have been drawn from measurements made at room temperature. To observe the effects of temperature on the decrement, the room-temperature measurements were extended to 70.0 °C and 120.0 °C. The pattern of the data including the effect of the pore fluid on the decrement, the frequency dependence, the pressure dependence, and the breakdown of the effective stress law continues at the higher temperatures. However, all other things being equal, the decrements are found to decrease as the temperature increases.

To examine the temperature dependence in detail, additional measurements were made at 10.0 °C intervals for a fixed external pressure of 45.0 MPa. Figure 11(a) shows the extensional decrement in brine-saturated Berea over a range of effective pressures. At 5.0 MPa, the first three odd harmonics are shown to illustrate the uniform decrease which occurs at all elastic wave frequencies. The trend over this relatively limited temperature range is roughly linear. For the remaining effective pressures only the first harmonic is shown in the interest of simplicity. There is a decrease in the fractional change of the decrement over the temperature range which indicates the decrement becomes relatively temperature independent at high effective stress. The torsional decrement in the brine-saturated sample shows a temperature dependence
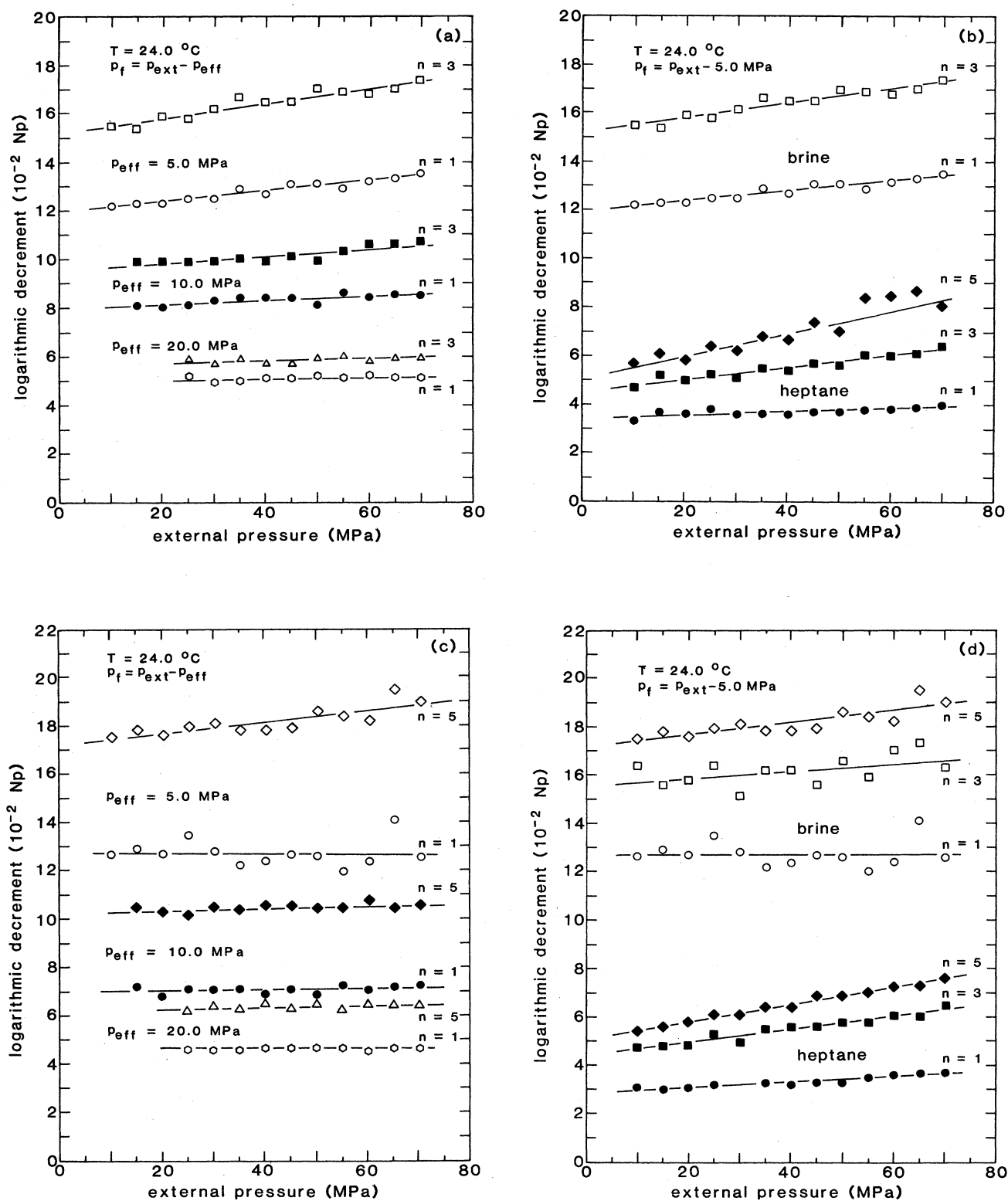
FIG. 10. Decrement for selected harmonics in saturated Berea vs the confining pressure applied to the sample for constant effective stress acting on the sandstone. All data for a temperature of 24.0°C. (a) Extensional mode with brine saturation for effective stresses of 5.0, 10.0, and 20.0 MPa. (b) Comparison between brine saturation and heptane saturation for the extensional mode at 5.0-MPa effective stress. (c) Torsional mode with brine saturation for effective stresses of 5.0, 10.0, and 20.0 MPa. (d) Comparison between brine saturation and heptane saturation for the torsional mode at 5.0-MPa effective stress.
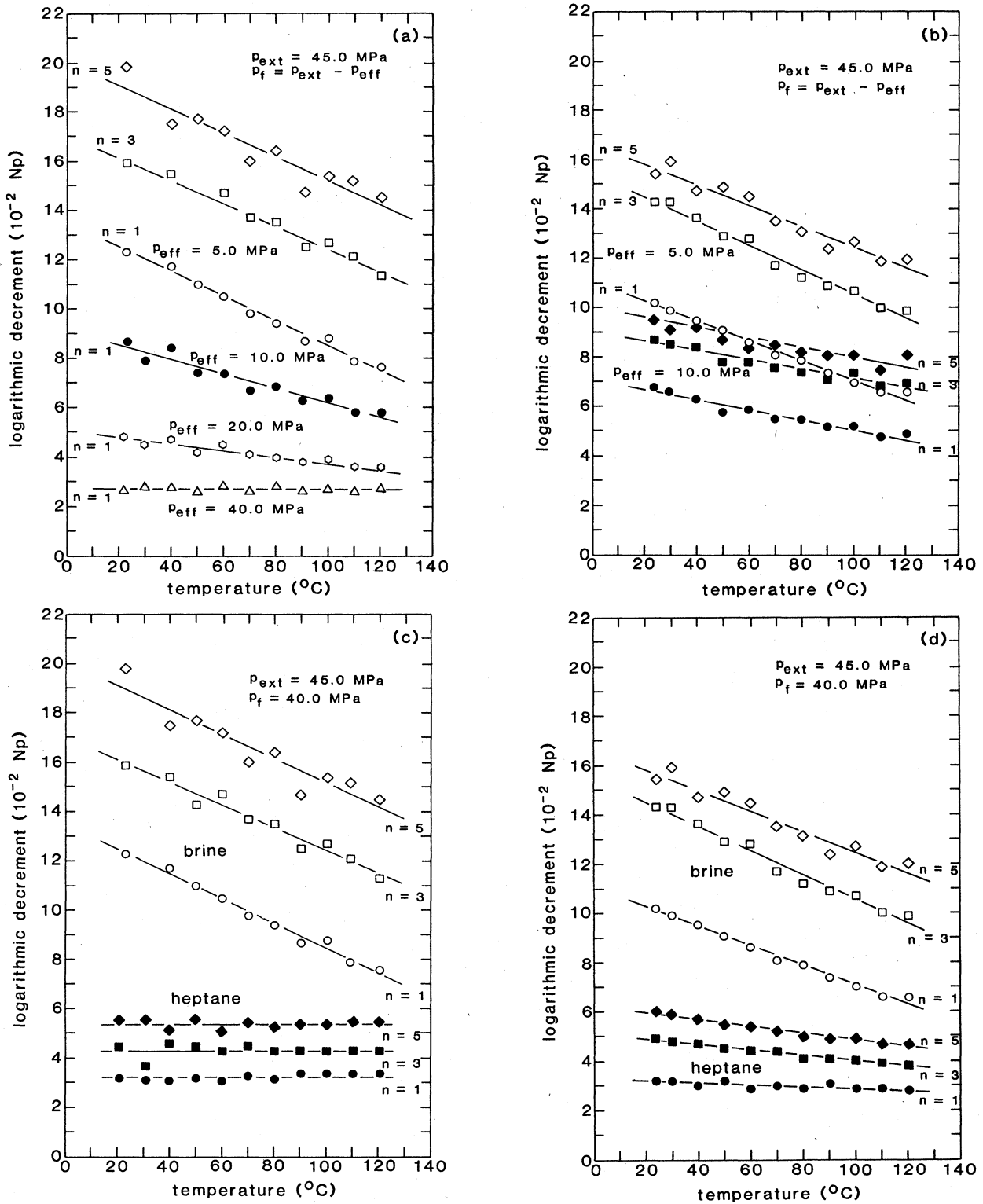
FIG. 11. Decrement for selected harmonics in saturated Berea vs the sample temperature for constant value of the effective stress acting on the sandstone. For all data, confining pressure applied to the sample fixed at 45.0 MPa. (a) Extensional mode with brine saturation. Three harmonics shown for effective stress of 5.0 MPa; for other effective stresses only first harmonic is shown. (b) Torsional mode with brine saturation. Three harmonics are shown for effective stresses of 5.0 and 10.0 MPa. (c) Comparison between brine saturation and heptane saturation for the first three odd harmonics of the extensional mode at 5.0-MPa effective stress. (d) Comparison between brine saturation and heptane saturation for the first three odd harmonics of the torsional mode at 5.0-MPa effective stress.

analogous to the extensional mode. In Fig. 11(b) the first three odd harmonics of the torsional decrement are plotted for effective pressures of 5.0 and 10.0 MPa. Since the trend had become evident, detailed data at higher effective stresses were not taken.

For the case of heptane saturation the temperature dependence is less pronounced. On the basis of the brine-saturated case, the largest changes would be expected at low effective stress. But a comparison in Fig. 11(c) of the extensional decrements at 5.0 MPa between the brine- and heptane-saturated cases shows little evidence of temperature dependence in the latter. On the other hand, a similar comparison for the torsional mode in Fig. 11(d) suggests the temperature dependence observed for the brine case is not particular to this pore fluid. The temperature dependence in the heptane-saturated sample is somewhat masked by the rather small value of the decrement.

IV. INTERPRETATION

All the above data imply that the pore fluid and geometric factors within the sandstone matrix control the attenuation. Comparison of the data on brine with those on heptane suggests a scaling law exists which predicts the attenuation once the correct pore fluid properties are stipulated. It is tempting to choose a list of pore fluid properties which can be expressed in terms of macroscopic observables. But existing theories which do so fall short of predicting the correct magnitude of the attenuation, with the possible exception of the theory proposed by Biot.[14] Johnston, Toksoz, and Timur[31] have calculated the attenuation from several popular theories for the particular case of the Berea sandstone. Biot's theory predicts the attenuation should have a frequency-squared dependence within the usual range of resonant rod experiments. This might explain a linear frequency-dependent component in the decrement if the attenuation is due in part to a Biot mechanism. Unfortunately, the Biot model contains no explicit provision for pressure- or temperature-dependent effects, so comparison over the range of the data presented here is difficult. In addition, the model seems to presume displacements in the fluid and sandstone matrix inconsistent with the small strain amplitudes used in the present measurements (and also characteristic of seismic wave propagation within the earth). For linear strains, $\Delta L/L < 10^{-6}$, and matrix grain-to-grain displacements must be of nearly atomic order.

An attractive alternative is the notion of the adsorption process which apparently controls the attenuation in very dry rock. The behavior seen in the present experiments on saturated rock may be an extension of similar experiments on vacuum dried or partially saturated sandstone.[5-7] In particular, Clark and co-workers report that fluids consisting of molecules with a high dipole moment produce significantly larger attenuation for the same mass of fluid adsorbed within the sandstone matrix than fluids with a low dipole moment. Further, these fluids when adsorbed in sufficient quantity produce an attenuation comparable in magnitude to that in saturated rock. These observations could very well justify the difference evident in the attenuation of the brine- and heptane-saturated samples.

If so, then the presence of the bulk fluid occupying the pore space in a saturated rock may not contribute significant additional attenuation. But the thermodynamic state of this fluid will affect any process taking place at the interface between the matrix grains and the fluid within the zone of adsorption. This may provide a partial explanation for the dependence of the decrement on the temperature and pore fluid pressure.

This viewpoint seems sustained by the frequency dependence of the attenuation. The measurements of Pandit and King[7] suggest that the frequency dependence reported in this work and in other measurements on sandstone[4,12] does not require that the rock be saturated. The nonlinear frequency dependence of the decrement may only indicate a modification of the basic process which operates in vacuum evacuated rock.

A comment should be made concerning the sites of the attenuation process. As noted, the logarithmic dependence of the decrement (and velocity) on the effective stress suggests that primarily pore openings of the smallest dimensions dominate the attenuation. Further, increasing temperature will have the effect of closing openings sensitive to small matrix dimensional changes. And the decrement does decrease with increasing temperature. But at high effective stress, say 60.0 MPa, the decrement for either pore fluid is becoming independent of pressure, as shown in Fig. 8. Presumably this implies that most of the smaller pore openings are closed. Comparing Fig. 8(b) to Fig. 7, the attenuation is still controlled by a fluid-related mechanism even at high effective pressure. Thus the magnitude of the attenuation must reflect to some extent the properties of large pore openings and, quite possibly, the effective surface area of the entire pore space.

If the frequency dependence illustrated in Fig. 9 is extended by linear extrapolation to seismic frequencies, a decrement is obtained which is effectively frequency independent through the seismic frequency band. This result sustains the common practice of using a "constant Q" attenuation in processing data on low-frequency elastic waves within the earth. Support for this interpretation comes from other reported measurements[12] of the extensional mode decrement in fluid-saturated sandstone and limestone. These measurements made at 100–250 Hz and again at 7–8 kHz show a difference in the decrement which depends on the effective stress in a manner similar to that shown in Fig. 9.

V. CONCLUSION

The measurements in this study provide a substantial basis for correlating the attenuation with lithologic and pore fluid properties through thermodynamic and elastic wave variables. Measurements on sandstone with only these two different fluids may indicate a pattern which is universal in character. But without a sustaining theory, these findings must be extended to other lithologic situations with caution. Unfortunately, present theories advanced to explain attenuation in rock appear to be inadequate to explain the variety of attenuation effects observed. And the trend of recent experimental observations indicates that it may be well to examine the mechanisms

which these theories propose. Theoretical progress would seem to require mechanisms based on fundamental physical and chemical interactions taking place between pore fluids and rock matrix grains. To aid this cause, additional experiments of the type presented here are being considered. Primarily, experiments will concentrate on rock types with practical application to geophysical exploration for hydrocarbon deposits. But experiments will continue to be designed to emphasize the general behavior of the attenuation process.

ACKNOWLEDGMENTS

APPENDIX: DESCRIPTION OF BEREA SANDSTONE

Petrographic descriptions of Berea sandstone are available in Mann and Fatt[21] and in Timur.[32] Briefly, Berea sandstone is a very light grey, moderately well-sorted, medium to fine-grained protoquartzite composed primari-

TABLE II. Porosity and permeability of selected samples of Berea sandstone. The porosity is the pore volume per unit volume of the sandstone. The permeability is defined for Darcy flow.

Sample	Pore fluid	Porosity	Permeability $(10^{-13}$ m$^2)$
28900-3-1	air-dry	0.211	9.1
28900-3-2	air-dry	0.216	9.1
26727-86-1	brine; heptane	0.219	8.4
27033-67-1	brine	0.210	5.5
27033-68-1	brine	0.223	9.6

ly of subrounded to irregular and embayed grains. The sandstone is well cemented with quartz and clay cements and has a fairly uniform intergranular porosity ranging locally from 19% to 22%. The stone used in the present experiment is believed to be from the Cleveland Quarries Company of Amherst, Ohio. The resonant rod samples were prepared from cores 7.62 cm in diameter and 150–200 cm in length. Some of the cores showed very faint traces of bedding normal to the core axis.

There was some concern as to the effect of the pore fluids and extreme thermodynamic conditions on the sandstone. So several samples were sectioned and the sections compared with virgin samples of the sandstone. Electron microscope photographs revealed no obvious changes. Routine porosity and permeability measurements gave results presented in Table II. The first two entries are for virgin samples. The remaining entries are for samples used in experiments, and the pore fluid used with the sample is indicated.

[1]H. Kolsky, *Stress Waves in Solids* (Dover, New York, 1963).

[2]B. R. Tittman, Rockwell International Science Center (Thousand Oaks, CA), Document SC5805.1SA, 1979 (unpublished).

[3]Kenneth Winkler, Amos Nur, and Michael Gladwin, Nature (London) **277**, 528 (1979).

[4]W. T. Born, Geophysics **6**, 132 (1941).

[5]B. R. Tittman, V. A. Clark, J. M. Richardson, and T. W. Spencer, J. Geophys. Res. **85**, 5199 (1980).

[6]V. A. Clark, B. R. Tittman, and T. W. Spencer, J. Geophys. Res. **85**, 5190 (1980).

[7]B. I. Pandit and M. S. King, Can. J. Earth Sci. **16**, 2187 (1979).

[8]William F. Murphy III, J. Acoust. Soc. Am. **71**, 1458 (1982).

[9]W. P. Mason, K. J. Marfurt, D. N. Beshers, and J. T. Kuo, J. Acoust. Soc. Am. **63**, 1596 (1978).

[10]M. N. Toksoz, D. H. Johnston, and A. Timur, Geophysics **44**, 681 (1979).

[11]Kenneth William Winkler, Ph.D. thesis, Stanford University, 1979.

[12]B. R. Tittman, H. Nadler, V. A. Clark, L. A. Ahlberg, and T. W. Spencer, Geophys. Res. Lett. **8**, 36 (1981).

[13]M. R. J. Wyllie, G. H. F. Gardner, and A. R. Gregory, Geophysics **27**, 569 (1962).

[14]M. A. Biot, J. Acoust. Soc. Am. **28**, 168 (1956).

[15]G. H. F. Gardner, M. R. J. Wyllie, and D. M. Droschak, J. Pet. Technol. **16**, 189 (1964).

[16]Amos Nur and J. D. Byerlee, J. Geophys. Res. **76**, 6414 (1971).

[17]David H. Johnston and M. Nafi Toksoz, *Seismic Wave Attenuation* (Society of Exploration Geophysicists, Tulsa, 1981), pp. 130–131.

[18]Terry Jones and Amos Nur, *53rd Annual International Meeting Expanded Abstracts* (Society of Exploration Geophysicists, Tulsa, 1983), p. 583.

[19]A. E. H. Love, *A Treatise on the Mathematical Theory of Elasticity* (Dover, New York, 1944).

[20]W. H. Somerton and M. A. Selim, J. Soc. Pet. Eng. **1**, 249 (1961).

[21]R. L. Mann and I. Fatt, Geophysics **25**, 433 (1960).

[22]M. T. Browne and J. R. Pattison, J. Appl. Phys. **8**, 452 (1957).

[23]James T. F. Kao and Riki Kobayashi, J. Chem. Phys. **47**, 2836 (1967).

[24]L. L. Pitaevskaya and A. B. Bilevich, Zh. Fiz. Khim. **44**, 1594 (1970) [Russ. J. Phys. Chem. **44**, 897 (1970)].

[25]G. S. Kell and E. Whalley, Philos. Trans. R. Soc. London **258**, 565 (1965).

[26]W. B. Nichols, H. H. Reamer, and B. H. Sage, Ind. Eng. Chem. **47**, 2219 (1955).

[27]Andrew Gemant, J. Appl. Phys. **11**, 647 (1940).

[28]John L. Everhart, W. Earl Lindlief, James Kanegis, Pearl G. Weissler, and Frieda Siegel, *Mechanical Properties of Metals and Alloys* (U.S. GPO, Washington, D.C., 1943), pp. 73 and 74.

[29]H. B. Huntington, in *Solid State Physics,* edited by F. Seitz and D. Turnbull (Academic, New York, 1958), Vol. 7, pp. 213–351.

[30]See AIP document No. PAPS-PLRAA-32-472-41 for 41 pages of tables of data. Order by PAPS number and journal reference from American Institute of Physics, Physics Auxiliary Publication Service, 335 East 45 Street, New York, NY 10017. The price is $1.50 for each microfiche (98 pages) or $5 for photocopies of up to 30 pages and $0.15 for each page over 30 pages. Airmail additional. Make checks payable to American Institute of Physics. This material appears in the monthly Current Physics Microform edition of all journals published by AIP, on the frames following this article.

[31]D. H. Johnston, M. N. Toksoz, and A. Timur, Geophysics **44**, 691 (1979).

[32]A. Timur, Geophysics **33**, 584 (1968).
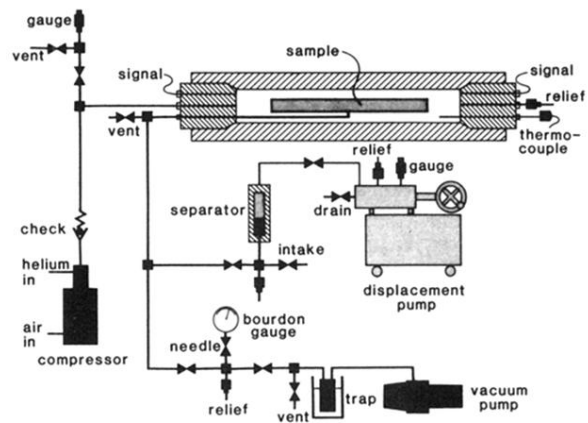
FIG. 1. Pressure apparatus used to subject sandstone samples to elevated temperatures and hydrostatic confining pressures and to regulate the sample pore fluid pressure.

FIG. 3. Cross section showing sample mounted within hollow cylinder of acoustic insulation. Sample is clamped by three mounting screws placed 120° apart on the circumference of an aluminum annulus which serves as the central section of the insulating cylinder. Only one of the mounting screws is visible in the section.